This is an open access article published under an ACS AuthorChoice License, which permits copying and redistribution of the article or any adaptations for non-commercial purposes.

Article

Cite This: Biomacromolecules 2019, 20, 2286−2294

pubs.acs.org/Biomac

Surface Activity and Foaming Capacity of Aggregates Formed between an Anionic Surfactant and Non-Cellulosics Leached from Wood Fibers

Wenchao Xiang,[†] Natalie Preisig,[‡] Christiane Laine,[§] Tuomo Hjelt,[§] Blaise L. Tardy,[†] Cosima Stubenrauch,*[,‡] and Orlando J. Rojas*[,†]

[†]Bio-Based Colloids and Materials, Department of Bioproducts and Biosystems, School of Chemical Engineering, Aalto University, P.O. Box 16300, Aalto, FI-00076 Espoo, Finland

[‡]Institut für Physikalische Chemie, Universität Stuttgart, Pfaffenwaldring 55, 70569 Stuttgart, Germany

[§]VTT Technical Research Centre of Finland Limited, P.O. Box 1000, FI-02044 Espoo, Finland

Supporting Information

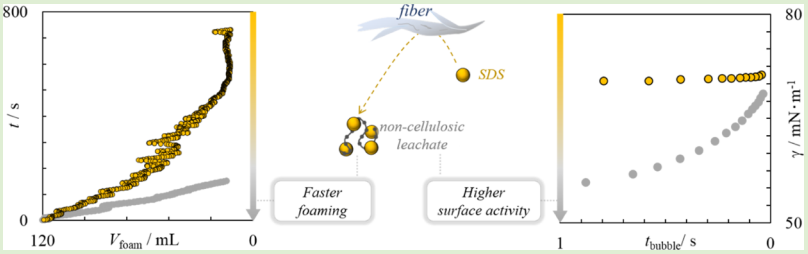

ABSTRACT: This study relates to the release of non-cellulosic components (cell wall heteropolysaccharides, lignin, and extractives) from swollen wood fibers in the presence of an anionic surfactant (sodium dodecyl sulfate, SDS) at submicellar concentrations. Highly surface-active aggregates form between SDS and the leached, non-cellulosic components, which otherwise do not occur in the presence of cationic or nonionic surfactants. The in situ and efficient generation of liquid foams in the presence of the leached species is demonstrated. The foaming capacity and foam stability, as well as the foam's structure, are determined as a function of the composition of the aqueous suspension. The results indicate that naturally occurring components bound to wood fibers are extractable solely with aqueous solutions of the anionic surfactant. Moreover, they can form surface-active aggregates that have a high foaming capacity. The results further our understanding of residual cell wall components and their role in the generation of foams.

INTRODUCTION

The unique properties of foams fulfill a wide range of purposes in nature and industry, for example, for the protection of embryo,[1] the dispersion of fibers in nonwoven manufacture,[2−5] the assembly of functional materials via templating,[6] the delivery of drugs,[7] and the formulation of household and food products.[8] In such applications, it is of critical importance to understand foam generation and stabilization. Air bubble generation in liquid media requires an energy input, which depends on the surface tension, γ, and the surface area of the generated air bubbles, ΔA.[9,10] For the generation and stabilization of foams, surfactants[11] are often used because they lower the surface tension thus facilitating the incorporation of bubbles. (Bio)polymers,[12] including proteins[13] and particles[14] are also used for foam generation and stabilization. Relevant for this study is the use of wood fibers and their main constituents for foam generation and stabilization. The main constituents in wood fibers refer to cellulose, which forms the structure of the cell walls and non-cellulosic components, mainly heteropolysaccharides (often termed as hemicelluloses),[15] extractives, and lignin.[4] These components have been incorporated in value-added materials[16−18] including lightweight structures.[2,19] Moreover, cellulosic nanomaterials have been proposed for the stabilization of aqueous foams.[7,15,20−23]

Using the components of the fibers' cell walls requires their isolation or fractionation with high energy and chemical costs. However, a different approach can be considered, namely, the treatment of fibers with surface-active agents, polymers, acid or base solutions by impregnation and diffusion.[24,25] Therein, the interactions between non-cellulosics and cellulose depend on hydrogen bonding and hydrophobic effects.[26,27] Typically, in neutral or weakly acidic conditions, non-cellulosics are negatively charged due to the presence of glucuronic acid and carboxylate groups. Thus, surfactants (anionic, cationic, or nonionic) can alter their net charge, surface chemistry, and colloidal stability. Most studies in this area deal with the interaction between negatively charged fibers and cationic or nonionic surfactants.[28] However, the interactions between

Received: February 17, 2019
Revised: April 19, 2019
Published: April 25, 2019

© 2019 American Chemical Society

DOI: 10.1021/acs.biomac.9b00243
Biomacromolecules 2019, 20, 2286−2294

negatively charged fibers and anionic surfactants have been studied only to a limited extent. Wood impregnation with microemulsions containing sodium dodecyl sulfate (SDS) was found to improve fiber wetting and the capillary penetration of SDS by adsorption onto hydrophobic sites.[29−34] It is thus reasonable to ask if an anionic surfactant enhances wood fiber accessibility, for example, by swelling and loosening its cell walls and if its interactions with non-cellulosic components lead to colloidally stable species or aggregates.

To address these questions, bleached pine fibers were used, which mainly consist of cellulose and small amounts of non-cellulosic components. The stability of the fibers suspended in water and in SDS solutions was studied, and the changes of the fiber's chemical composition were determined. The interaction between SDS and the non-cellulosics was examined by surface tension (static and dynamic) and by analyzing the composition of the system. Furthermore, the foaming capacity of the non-cellulosic fraction leached to the aqueous phase after treatment with SDS was elucidated. Finally, we took advantage of the interaction between SDS and the non-cellulosics and evaluated the foam properties of wood fiber dispersions in the presence of the surfactant.

EXPERIMENTAL SECTION

Materials. SDS (Sigma-Aldrich, purity ≥99.0%) and *n*-dodecyl-*β*-D-maltoside, *β*-$C_{12}G_2$ (Glycon, purity >99.5%) were used as received. Dodecyltrimethylammonium bromide, C_{12}TAB (BioXtra, purity ∼99%), was purified thrice by recrystallization. Reference softwood hemicellulose was extracted from commercial softwood Kraft pulp (Metsä Fibre) treated by 2.5 M NaOH and ultrafiltrated at 50 °C (LabStak M20, Alfa Laval AB, Sweden), as described elsewhere.[35] Never dried, bleached pine Kraft fibers (BKP) were produced and supplied by the Äänekoski Mill of Metsä Fibre, Finland. The fibers were washed and filtered extensively with 5 L batches of MQ water to eliminate any residual chemicals or components dissolved from the bleaching filtrate, which may have attached to the fibers during drying. The process was repeated (at least 10 times) until a conductivity of the aqueous filtrate reached a value <1.1 μS/cm in the last two cycles. The composition of the obtained, washed fibers is shown in Table S1, following Soxhlet extraction, hydrolysis, and pulse amperometric detection. In additional experiments, we used nonchemically treated, unbleached softwood thermomechanical fibers (TMP) (Sappi's Kirkniemi Mill, Finland) and dissolving grade fibers (DP), disintegrated from cotton linters and sourced from Milouban M.C.P., Ltd (see Tables S2 and S3 for the respective composition). High-grade nylon meshes were obtained from Finntex.

Leachate from the Fiber's Cell Wall. The purified, never dried fibers were firstly dispersed in MQ water (35 g) by vigorous hand shaking (1 min), and then 10 g of SDS (31.5 mM) was added. The final fiber content in the 45 g suspension was 0.3 wt %. After gentle mixing for 1 min, the suspension was filtered through the nylon mesh (pore diameter of 1 μm) that retained the fibers. The filtrate, containing surfactant and leachate from the fibers, was collected for use in further experiments. Note that the nylon membrane was thoroughly washed with ethanol and MQ water before use. The absence of any extractable materials or contaminants was verified by surface tension measurements using MQ and SDS (0.7 mM) solution filtered through the membrane.

The fibers retained in the nylon membrane were gently pressed by hand to avoid bubble generation while the filtrate, herein referred to as $Leachate_{0.7mM\ SDS}$, was collected for further analyses. The experiments involved washing/filtration cycles in which the fibers that remained on the nylon membrane were collected and redispersed repeatedly (five times) in 0.7 mM SDS solution (to obtain 45 g dispersions). The $Leachate_{0.7mM\ SDS}$ solutions obtained from the five dispersion or leaching cycles were collected for further studies. In the same manner, $Leachate_{MQ}$ was obtained from fibers dispersed in MQ water, in the absence of SDS. The same protocols were applied for the cationic and nonionic (C_{12}TAB and *β*-$C_{12}G_2$) surfactant solutions.

Static Surface Tension. To explore the effect of dispersion cycles, the static surface tension γ (21.5 ± 0.2 °C) of $Leachate_{0.7mM\ SDS}$ and $Leachate_{MQ}$ was measured after each cycle using a KSV Sigma 70 force tensiometer equipped with a Wilhelmy platinum plate. The γ of MQ water and pure 0.7 mM SDS solution was used as reference. The static surface tension of $Leachate_{SDS}$ obtained from BKP fibers at different SDS concentrations was measured. The surface activity of BKP fibers dispersed in SDS solutions at concentrations below, at, and above the critical micelle concentration (cmc_{SDS}) was assessed and compared with that of the corresponding leachate. The static surface tension measurements were conducted for at least 20 min with a steady plateau in surface tension of 5 min.

Dynamic Surface Tension. The dynamic surface tension ($\gamma_{dynamic}$) of $Leachate_{0.7mM\ SDS}$ solutions was measured using a KSV BPA-800P bubble pressure tensiometer using a capillary of 0.13 mm radius. SDS was used at three different concentrations, namely, 0.083 cmc_{SDS}, 1 cmc_{SDS}, and 8.3 cmc_{SDS}. The $\gamma_{dynamic}$ measurements were performed at 21.8 °C for 15−50 min until reaching a surface tension plateau as a function of bubble lifetime. The experimental time (15−50 min) is the time spent by the gas sensor in the tensiometer (a) to change gas flow, which is for generating bubbles with different lifetimes and (b) to establish the change interval between different gas flows. The bubble lifetime is the time interval from bubble generation to its hemispherical size. The surface tension was plotted as a function of bubble lifetime with 1 s resolution in this study. For comparison, the dynamic surface tension of MQ, $Leachate_{MQ}$, and pure SDS solutions at different concentrations was also recorded. The $\gamma_{dynamic}$ of the leachate obtained from cationic (C_{12}TAB) and nonionic (*β*-$C_{12}G_2$) surfactant solutions at different concentrations was also measured. Only BKP fibers were utilized in the dynamic surface tension experiments.

UV−Vis Spectroscopy and Attenuated Total Reflection−Fourier Transform Infrared Spectroscopy (ATR−FT-IR). The presence of soluble lignin content in the leachates was examined by measuring the absorbance at wavelengths between 200 and 1000 nm using a UV−vis spectrophotometer (UV-2550, Shimadzu, Kyoto, Japan). The absorbance intensity at 205 nm was used to qualitatively compare the lignin content. Hemicelluloses were identified in freeze-dried leachates using infrared spectroscopy (Nicolet 380 FT-IR) at 500−4000 cm^{-1} with the single-reflection diamond attenuated total reflection (ATR) accessory (smart orbit). The background signal was collected before measurements by running 64 scans in air.

Sample Preparation for Foam Experiments. To study the role of SDS concentration on foam properties, in the presence or absence of fibers, the following samples were prepared: (1) SDS solutions at a concentration below, at, and above the cmc_{SDS} (0.7, 8.4, and 70 mM); (2) aqueous fiber dispersions (0.3 wt %) in the presence of 0.7, 8.4, and 70 mM SDS; and (3) suspensions of $Leachate_{SDS}$ generated in situ from the respective samples in (2). Specifically, for the preparation of samples in (2), 70 mL of BKP fibers was dispersed in double-distilled water. Then, right before foam measurements, a certain volume of the SDS stock solution (315 mM) and double-distilled water were added to the dispersion so that its final volume was 90 mL. The BKP fiber content was fixed at 0.3 wt %, while the SDS concentration was 0.7, 8.4, or 70 mM. Before the foam experiments, the given fiber dispersion in SDS was kept under gentle magnetic stirring for 1 min to ensure homogeneous mixing while avoiding bubble formation. For the preparation of samples (3), the $Leachate_{SDS}$ was collected by filtering the respective system using a clean nylon membrane, as described before. Double-distilled water was used throughout the foam experiments, which are described in detail next.

Aqueous Foam Generation and Evaluation. Foam properties (foamability and foam stability) were followed by using a FoamScan unit (Teclis, France).[36] The initial liquid volume was kept at 60 mL and nitrogen gas was injected from the bottom of the column at a rate of 84 mL/min using a porous fritted glass disc (average pore diameter in the 41−100 μm range). The foamability was evaluated by recording the time taken to reach a foam volume V_{foam} = 120 mL. Once the gas

DOI: 10.1021/acs.biomac.9b00243
Biomacromolecules 2019, 20, 2286−2294

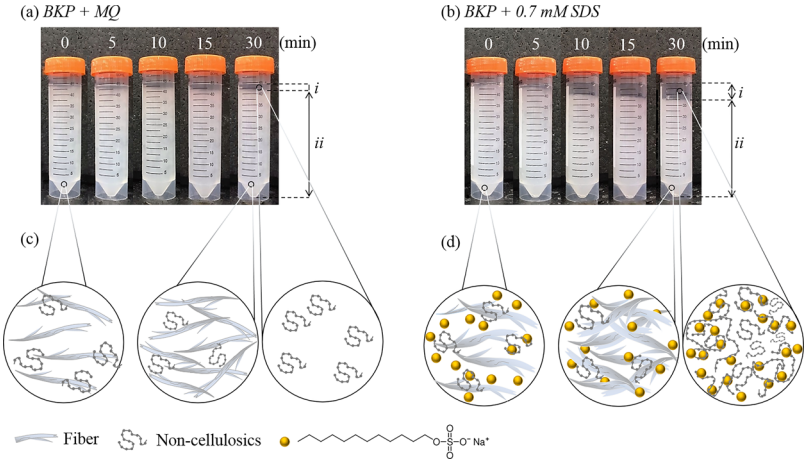

Figure 1. Photographs of 0.3 wt % (BKP) fibers dispersed in (a) MQ water and (b) 0.7 mM SDS solution 0, 5, 10, 15, and 30 min after mixing. Note that the phase separation can be followed by observing the upper clear phase (i) that develops with time relative to the bottom phase (ii). Schematic illustrations of the time evolution of the fiber dispersions in MQ water and 0.7 mM SDS are included in (c,d), respectively (the legend for the different components in the bottom is not to scale).

flow was stopped, the foam stability was assessed by recording the changes of the foam volume (V_{foam}) and of the liquid fraction (ε) as a function of time. For this purpose, a charge-coupled device (CCD) camera and electrodes located inside the *FoamScan* column, respectively, were used. The evolution of the bubble size was followed with a cell size analysis (CSA) camera positioned at the wall of the column. The maximum foaming and total experimental time were set at 2000 and 2200 s, respectively. At least two foaming tests were run for each sample. The images obtained from the CSA camera were analyzed with the freeware program *ImageJ* to obtain a water-free skeleton image after reducing the dark areas of the surface plateau borders into lines of one-pixel width. Then, the skeletonized images were analyzed using the CSA software of the *FoamScan* unit. The bubble size $\langle r \rangle$ and size distribution were determined in repeated experiments and the standard deviations are reported.

RESULTS AND DISCUSSION

Fiber Leachate Caused by SDS. We first conducted very simple experiments to check whether SDS extracts non-cellulosics from the cell walls of wood fibers. As expected, BKP fibers dispersed in MQ water gradually separate into two phases, Figure 1a,c. The upper phase "i" contains non-cellulosics leached from fibers, while the lower phase "ii" contains fibers and traces of non-cellulosics dispersed in the entire aqueous medium. The composition in these two phases is confirmed further below. When SDS is added to the aqueous medium (at submicellar conditions, e.g., in the presence of SDS unimers), the amount of the top phase "i" (Figure 1b) is larger than that of the top phase "i" without SDS (Figure 1a). To rule out the effect of ionic strength, we performed an experiment with 0.7 mM NaCl, which leads to the same results as the experiment with MQ water (images not shown). It is plausible that SDS causes the release of non-cellulosics by reducing the interfiber repulsion, leading to the formation of (a) a denser phase "ii", which contains mainly fibers and traces of aggregates between non-cellulosics and SDS, that is $Leachate_{0.7mM\ SDS}$, as well as (b) phase "i" containing solely $Leachate_{0.7mM\ SDS}$ (Figure 1d). The release of non-cellulosics is suggested to be a consequence of three phenomena: (a) the adsorption of SDS onto fibers via hydrophobic interactions;[29−34,37] (b) the swelling of the fiber structures,[30,31] presumably due to the penetration of SDS into the cellulosic network[30,31] and the charge-dipole attraction between the anionic sulfate group of SDS and hydrogens of water molecules;[38] and (c) the detachment of non-cellulosics from fibers' cell walls and, subsequently, the formation of aggregates with SDS (Figure 1d, upper phase), possibly via ion/charge-dipole interactions.[39,40] It is reasonable to expect that upon the leaching of charged non-cellulosics from fibers, an osmotic pressure gradient is generated between the interfiber cell walls and the dispersion medium,[41] which may induce depletion flocculation of fibers. The complex nature and identity of the non-cellulosics remain as an unresolved challenge, which may require sophisticated analytical approaches. Instead, we focused our investigation on the consequences of the release of non-cellulosics induced by SDS and the formation of the respective aggregates. This is expected to provide grounds for further studies on the interaction between SDS and non-cellulosics and related phenomenological aspects.

To determine the composition of the leachate, we used ATR−Fourier transform infrared spectroscopy (FT-IR), UV−vis, and carbohydrate analyses. Negatively charged hemicelluloses, which are soluble in water, are expected to be one of the non-cellulosic components leached from the BKP fibers. To test this hypothesis, $Leachate_{MQ}$ and $Leachate_{0.7mM\ SDS}$ were obtained from the fibers after five dispersion/washing cycles, followed by freeze-drying and ATR−FT-IR characterization. By comparing the respective ATR−FT-IR spectra with those obtained from SDS and reference hemicelluloses,[35] the characteristic peaks of hemicellulose are identified for both $Leachate_{MQ}$ and $Leachate_{0.7mM\ SDS}$. The absorbances of $Leachate_{MQ}$ and $Leachate_{0.7mM\ SDS}$ at 3355, 1040, and 897 cm^{-1} (Figure 2a−c) are assigned to hemicelluloses. These characteristic peaks correspond to the O−H (3355 cm^{-1}) and the C−O (1040 cm^{-1}) bond stretching of the ether groups and the β-1,4 glycosidic bond stretching (897 cm^{-1}).[42] Additionally, the peak at 1215 cm^{-1} is assigned to the stretching of skeletal vibration of S−O in SDS,[43] which is found in the spectra of neat SDS and $Leachate_{0.7mM\ SDS}$. The ATR−FT-IR results confirm the presence of hemicelluloses in $Leachate_{MQ}$ and $Leachate_{0.7mM\ SDS}$. However, released lignin in the leachate cannot be ruled out because hemicelluloses are associated with lignin forming lignin−carbohydrate complexes (LCC),[44] which are difficult to separate into the individual components.[45−49] In fact, the presence of lignin in $Leachate_{MQ}$ and $Leachate_{0.7mM\ SDS}$

DOI: 10.1021/acs.biomac.9b00243
Biomacromolecules 2019, 20, 2286−2294

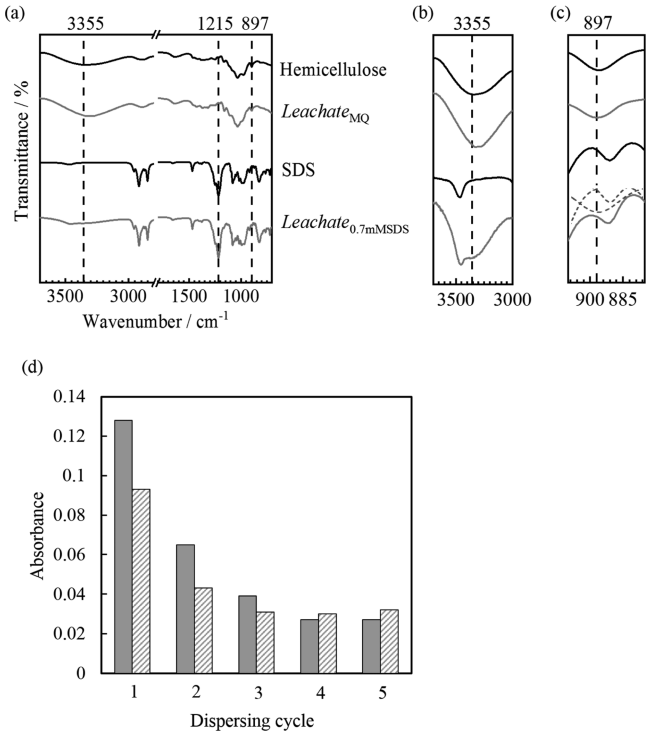

Figure 2. (a) ATR−FTIR spectra (500−4000 cm^{-1}) of a reference hemicellulose, pure SDS, *Leachate*$_{MQ}$, and *Leachate*$_{0.7mM\ SDS}$ obtained from BKP fibers. (b) Characteristic peaks at 3355 cm^{-1} for the reference hemicellulose and *Leachate*$_{MQ}$ are magnified 3×, while those assigned to SDS and *Leachate*$_{0.7mM\ SDS}$ are magnified 10×. (c) Characteristic peak at 897 cm^{-1} for the reference hemicellulose and *Leachate*$_{MQ}$ (magnified 5×) and for SDS and *Leachate*$_{0.7mM\ SDS}$ (magnified 10×). The peak of *Leachate*$_{0.7mM\ SDS}$ was deconvoluted (dash lines) to highlight the peak at 897 cm^{-1}. (d) Bar plot corresponding to the absorbance intensity (205 nm) from the UV−vis spectra corresponding to *Leachate*$_{MQ}$ (filled bars) and *Leachate*$_{0.7mM\ SDS}$ (patterned bars) obtained from BKP fibers after the different dispersion cycle.

obtained from BKP fibers over five dispersion cycles is confirmed by the UV−vis absorbance data (205 nm), Figure 2d. Because residual extractives, such as fatty acids and sterols, may also be present in LCC, the presence of extractives in leachate was examined using carbohydrate analyses, for example, by comparing the composition of fibers before and after removing leachate. From the data in Table S1, it is clear that the leachate from the BKP fibers contained hemicellulose, lignin, and extractives.

After five dispersion cycles, using either MQ water or 0.7 mM SDS solution, a reduction in the amount of residual extractives in the solid phase (the BKP fibers) was observed, in agreement with the presence of extractives in *Leachate*$_{MQ}$ and *Leachate*$_{0.7mM\ SDS}$, as previously hypothesized. The aggregates present in *Leachate*$_{MQ}$ and *Leachate*$_{0.7mM\ SDS}$ were further studied with dynamic light scattering (see the autocorrelation functions in Figure S1a). The longer decay time for *Leachate*$_{0.7mM\ SDS}$ indicates a larger hydrodynamic size compared to the aggregates in *Leachate*$_{MQ}$ (Figure S1b). In conclusion, the results clearly show that non-cellulosics (hemicellulose, lignin, and extractives) are present in the leachate solutions. However, it is difficult to determine whether lignin and the extractives in the leachate are solubilized as single components or bound to hemicelluloses. Carboxylic and other groups in lignin are very likely engaged in the formation of LCC.[50] Similarly, the extractives are poorly soluble in water, and it is possible that they also bind to the hemicelluloses in the leachate.

The results discussed so far suggest that SDS extracts non-cellulosic components from the BKP fibers, which form aggregates with the surfactant in the aqueous medium. However, several questions exist, such as (a) the nature of the interactions between SDS and non-cellulosics; (b) the structure of the aggregates and their composition in the molar ratio, for example, SDS unimers versus non-cellulosics; and (c) the role of sodium counterions and the hydrocarbon groups of SDS. These points remain open for further studies. Here, we want to exploit the non-cellulosics in general and the surfactant/non-cellulosics aggregates in particular as foaming agents. For this purpose, we expand our studies by comparing the surface activity, the foaming capacity, and the foam stability of suspensions containing fiber and leachate, or leachate alone, with those of the respective SDS solutions.

Surface Activity of *Leachate*$_{SDS}$. Figure 3a compares the surface tension isotherm of SDS solutions (filled symbols) with that of *Leachate*$_{SDS}$ after having the BKP fibers exposed to SDS solutions of the corresponding concentration (open, gray symbols). The surface tension isotherm of SDS solutions at 22.1 °C is in line with those reported in the literature.[51] The solutions of *Leachate*$_{SDS}$ obtained after being exposed to SDS at submicellar concentrations have lower surface tension values than those of the respective pure SDS solution (Figure 3a). The enhanced surface activity of leachate is more apparent in the presence of SDS (Figure 3b, pattern-filled bars) than in MQ water (Figure 3b, filled bars). By increasing the number of dispersing cycles, one can see that the surface tension difference between leachate and the corresponding solutions (SDS or MQ water) decreases (Figure 3b). This observation indicates that the amount of non-cellulosics extracted from fibers exhausts progressively over dispersing cycles. Given the extremely low concentrations, our gravimetric and carbohydrate analyses were not sensitive enough to quantify the concentration of non-cellulosics in the leachates (Table S1). However, their presence is clearly evidenced from the surface tension isotherms of *Leachate*$_{MQ}$ and *Leachate*$_{0.7mM\ SDS}$ obtained after a given number of dispersion cycles, as discussed above.

Fibers other than BKP, namely, "dissolving grade" (DP) and TMP fibers, which widely differ in their composition (Tables S2 and S3), were used to further elucidate the effect of leached non-cellulosics obtained over five dispersion cycles (*Leachate*$_{MQ}$ and *Leachate*$_{0.7mM\ SDS}$) on aggregate formation and surface activity (Figures S2 and S3). Detailed discussions can be found in the Supporting Information.

Taken all together, there is a clear evidence of the presence of non-cellulosics that interact with the anionic surfactant and increase the air/water interfacial activity of *Leachate*$_{SDS}$. This conclusion is relevant for the application of natural components released in situ from fibers via a simple surfactant treatment, such as their use for the generation of liquid foams as will be shown further below.

In addition to the static surface tension, we also measured the dynamic surface tension of SDS solutions at three concentrations, namely, 0.7 mM = 0.083 cmc_{SDS}, 8.4 mM = cmc_{SDS}, and 70 mM = 8.3 cmc_{SDS}. Because $\gamma_{dynamic}$ is time-dependent and relates to the diffusion and adsorption rates in the system, we also evaluated the efficiency of the respective

DOI: 10.1021/acs.biomac.9b00243
Biomacromolecules 2019, 20, 2286−2294

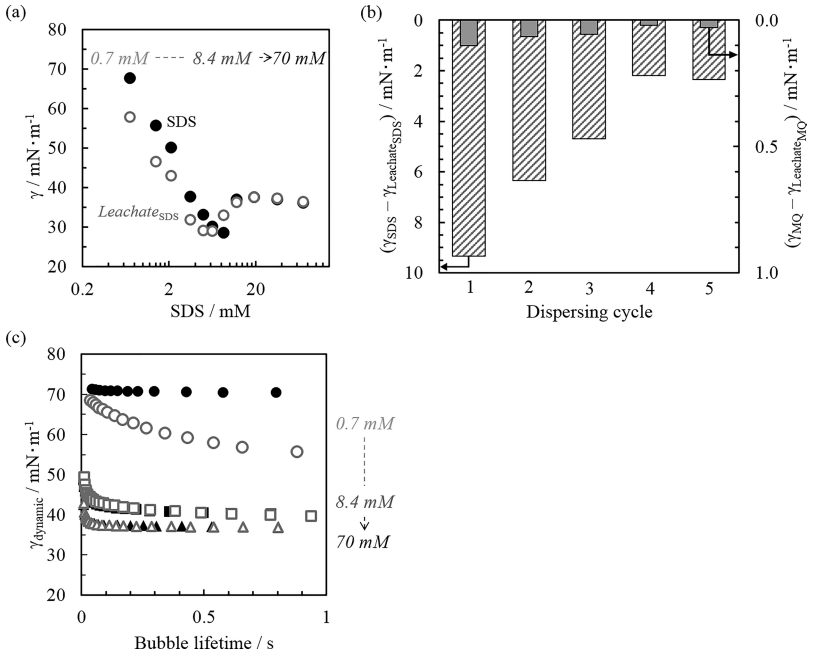

Figure 3. (a) Surface tension, γ, as a function of SDS concentration for pure SDS solutions (filled symbols) and $Leachate_{SDS}$ obtained from the first dispersion cycle using BKP fibers (open symbols). (b) $(\gamma_{SDS} - \gamma_{Leachate_{SDS}})$ in 0.7 mM SDS solutions (left y-axis for patterned bars) and $(\gamma_{MQ} - \gamma_{Leachate_{MQ}})$ (right y-axis for solid bars) as a function of dispersion cycles. (c) Dynamic surface tension, $\gamma_{dynamic}$, as a function of bubble lifetime for pure SDS solutions (filled symbols) and $Leachate_{SDS}$ from BKP fibers (open symbols). The SDS concentrations studied were 0.7 mM (circles), 8.4 mM (squares), and 70 mM (triangles).

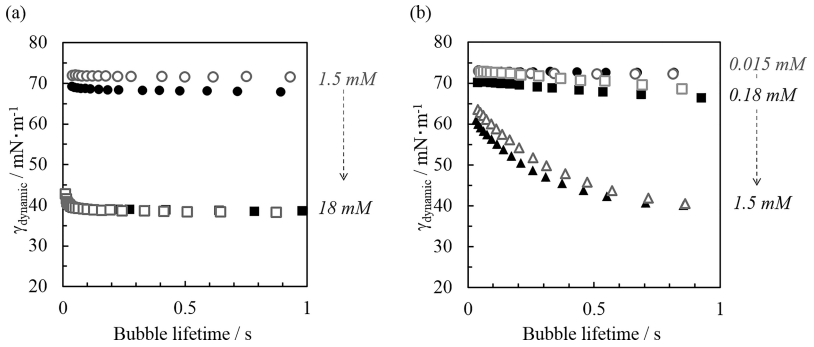

Figure 4. (a) Dynamic surface tension, $\gamma_{dynamic}$, as a function of bubble lifetime for pure C_{12}TAB solutions (filled symbols) and $Leachate_{C_{12}TAB}$ from BKP fibers (open symbols). The concentration of C_{12}TAB was varied from 1.5 mM (circles) to 18 mM (squares). (b) $\gamma_{dynamic}$ as a function of bubble lifetime for pure β-$C_{12}G_2$ solutions (filled symbols) and $Leachate_{C_{12}G_2}$ from BKP fibers (open symbols). The concentration of β-$C_{12}G_2$ varied from 0.015 mM (circles) to 0.18 mM (squares) and 1.5 mM (triangles).

leachates in reducing the surface tension. We investigated whether SDS unimers diffuse faster to the air/water interface than the surface-active aggregates in $Leachate_{SDS}$ (see Figure 3c for the $\gamma_{dynamic}$ of SDS (filled symbols) and $Leachate_{SDS}$ (empty, gray symbols) as a function of bubble lifetime). At a SDS concentration < cmc_{SDS} (Figure 3c, circles), SDS unimers reach an equilibrium in $\gamma_{dynamic}$ ($\gamma_{dynamic,eq}$) very rapidly (~0.05 s). In contrast, $Leachate_{0.7mM\ SDS}$ takes longer time (~1 s) to reach $\gamma_{dynamic,eq}$. The shorter diffusion time of $Leachate_{0.7mM\ SDS}$ is expected owing to the hydrodynamic size of the aggregates compared to SDS unimers (Figure S1). The $\gamma_{dynamic,eq}$ of $Leachate_{0.7mM\ SDS}$ is similar to that obtained from static measurements (Figure 3a). Upon increasing SDS concentration to the cmc_{SDS} and above (8.3 cmc_{SDS}), the $\gamma_{dynamic}$ of both SDS and $Leachate_{SDS}$ present a similar trend, indicating that SDS dominates the measured surface tension (an observation i.e., corroborated later from foam experiments). Additionally, $\gamma_{dynamic,eq}$ at high SDS concentrations is reached rapidly as a result of the readily available SDS unimers in the system. We note that the surface tensions of $Leachate_{SDS}$ at SDS concentrations of 0.7, 8.4 and 70 mM (Figure 3a) are similar to those in the presence of BKP fibers (Table S4), indicating that the leaching of non-cellulosics mainly depends on SDS concentration (Figure 3b) and less on the contacting time.

The effect of surfactants in extracting non-cellulosics from wood fibers was tested by comparing $\gamma_{dynamic}$ of solutions containing the pure surfactant and those obtained after contact with the fibers. The surfactants chosen had nonpolar groups of the same length as SDS, namely, the cationic surfactant C_{12}TAB and the nonionic surfactant β-$C_{12}G_2$, which were tested at concentrations below, at, and above the respective

DOI: 10.1021/acs.biomac.9b00243
Biomacromolecules 2019, 20, 2286−2294

cmc (Figure 4). We noted no reduction in the surface tension of the leachate solutions obtained from C_{12}TAB or β-$C_{12}G_2$. This observation highlights the unique role of the anionic surfactant, which supports our hypothesis on leachate formation, as discussed earlier. Namely, SDS-induced fiber swelling due to hydrophobic effects[30,31] and interactions with the polar group of SDS[38] that increase the accessibility of non-cellulosics and their release from fibers.[39,40] Such effects may not be relevant when cationic or nonionic surfactants are applied at submicellar concentration. In these cases, favorable electrostatic and hydrogen bonding interactions may exist, and the overall effect is that leaching does not occur or cannot be quantified. To the best of our knowledge, the role of SDS in leaching non-cellulosics from wood fibers and the subsequent formation of surface-active aggregates is reported here for the first time.

Effect of *Leachate*$_{SDS}$ on Foam Properties. Substances with low surface tension and fast adsorption dynamics at the air/water interface are usually good foaming agents.[52,53] Given the lower surface tension and fast diffusion (though *Leachate*$_{0.7mM\ SDS}$ is slower than SDS unimers) of *Leachate*$_{SDS}$ compared to those of pure SDS (Figure 3c), it is interesting to test whether *Leachate*$_{SDS}$ influences the foaming properties. To elucidate whether the shape-anisotropic and relatively flexible fibers affect the foam properties, the foamability and the foam stability of BKP fiber dispersions in the presence of SDS (0.7, 8.4, and 70 mM) are compared to those of corresponding pure SDS solutions or *Leachate*$_{SDS}$ prepared at the given SDS concentrations.

Figure 5a shows a typical *FoamScan* experiment, including foam generation (time up to 0 s, Figure 5a,I) and foam (de)stabilization (time >0 s, Figure 5a,II). The time required for generating 120 mL foam was used to determine the foamability, while the time evolution of V_{foam} was used as a measure for foam stability. As can be seen from Figure 5b–d, fiber-loaded foams in the presence of SDS and *Leachate*$_{SDS}$ exhibit similar foamability and foam stability at the SDS concentrations studied. The enhanced foam stability of fiber-loaded foams compared to foams produced from *Leachate*$_{0.7mM\ SDS}$ or 0.7 mM SDS is caused by an artifact in imaging, as can be seen in Figure S4. Thus, the presence of fibers does not change the foaming capacity and foam properties compared to foams generated with *Leachate*$_{SDS}$ alone.

The foaming capacity of *Leachate*$_{SDS}$ is found to be SDS concentration-dependent. At a SDS concentration lower than cmc_{SDS} ($c < cmc_{SDS}$), the foamability of *Leachate*$_{0.7mM\ SDS}$ and fiber-loaded SDS solution (0.7 mM) appear to be higher than those observed for the pure SDS solution at 0.7 mM (Figure 5b). The shortest time to reach V_{foam} = 120 mL (foaming time) is measured for *Leachate*$_{0.7mM\ SDS}$ (159 s) (Video S1), followed by the foaming time of fiber-loaded SDS 0.7 mM (217 s) and that of the pure 0.7 mM SDS solution (734 s) (Video S2). Together with the surface tension data (Figure 3a,c), the results reveal possible synergies between SDS with non-cellulosics in *Leachate*$_{0.7mM\ SDS}$ as well as their generation in situ from the dispersions containing the fibers in SDS solution.

Because of the low concentration of the surface-active aggregates in *Leachate*$_{0.7mM\ SDS}$, the newly created air/liquid interfaces are not stable enough to support the capillary suction against drainage. Therefore, once the gas flow stops, the foam volume collapses rapidly. Evidently, compared to those observed at a submicellar concentration, at a high-

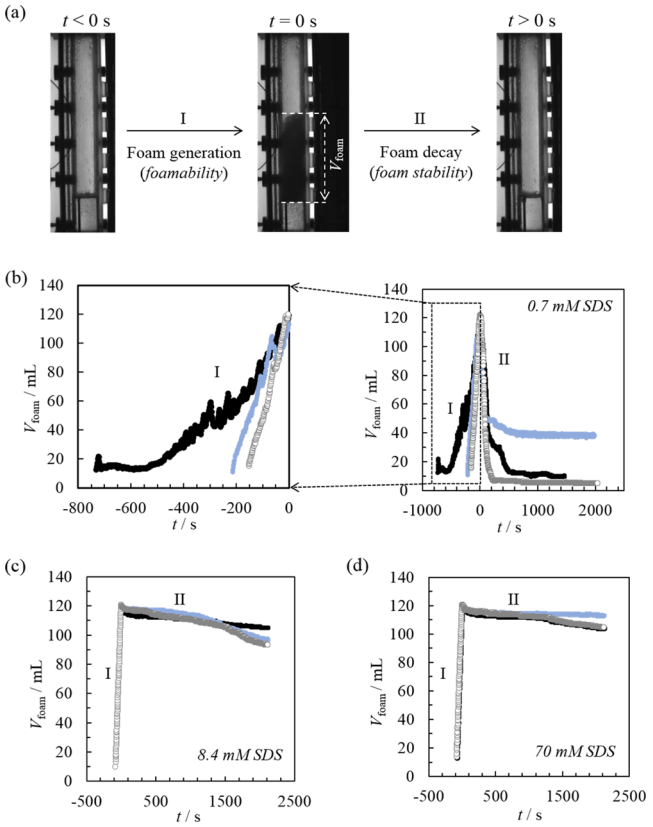

Figure 5. (a) CCD images of a foam column showing (I) foam generation (dark phase in the column) and (II) foam decay. (b–d) Changes in the foam volume (V_{foam}) as a function of time for pure SDS solutions (black symbols), fiber-loaded SDS solutions (blue symbols), and *Leachate*$_{SDS}$ (empty-gray symbols). The concentration of SDS used corresponds to (b) 0.7, (c) 8.4, and (d) 70 mM. The fiber loading in the respective media was fixed at 0.3 wt %. t = 0 s refers to the time at which the foam volume reached 120 mL, after which the gas flow was stopped. In (b), the different evolution of foam height at $t < 0$ is highlighted in a magnified view of the profiles, shown on the left.

enough concentration of SDS ($c \geq cmc_{SDS}$), the foamability and foam stability are higher for all the systems, including the pure SDS solutions, the fiber-loaded SDS dispersions, and the *Leachate*$_{SDS}$ (Figure 5c,d). The results indicate the requirement of a sufficient amount of the surface-active agent to achieve fast foaming and good foam stability. Figure 5c,d show no substantial differences in the foamability and foam stability of SDS solutions, fiber-loaded SDS dispersions, and *Leachate*$_{SDS}$, suggesting the dominant role of SDS in foam properties at $c \geq cmc_{SDS}$.

The decay of foam volume is not the only a measure for foam stability. Major factors influencing foam stabilization include gravity-driven drainage, coalescence due to film rupture, and coarsening via gas diffusion. Drainage is measured by monitoring the foam's liquid fraction, ε, over time, as shown in Figure 6a,b. The results for foams generated with 0.7 mM SDS are not included in the following discussion due to limitations in the statistical analysis of the air bubbles captured by the CCD camera, Figure S4. At $t < 400$ s, the liquid fraction is about the same and decays at the same rate for the SDS solution, fiber-loaded SDS dispersion, and the *Leachate*$_{SDS}$ (Figure 6a,b). The presence of fibers in the SDS solution does not inhibit drainage. Upon drainage, the foam films

DOI: 10.1021/acs.biomac.9b00243
Biomacromolecules 2019, 20, 2286–2294

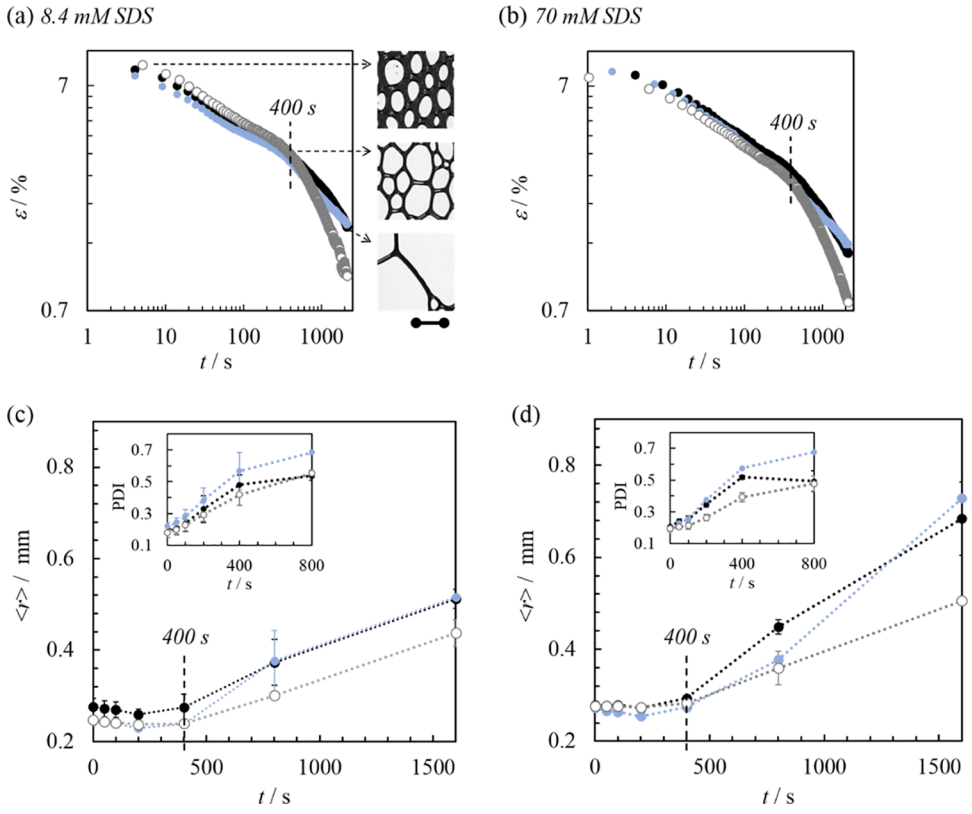

Figure 6. (a,b) Changes in the foam liquid fraction (ε) as a function of time for pure SDS solutions (black), fiber-loaded SDS dispersion (blue) and $Leachate_{SDS}$ (empty, gray symbols). The scale bar below the CSA pictures corresponds to 0.25 mm. (c,d) Evolution of the arithmetic average bubble size $\langle r \rangle$ of SDS solutions (black), BKP fiber dispersion in SDS (blue), and its $Leachate_{SDS}$ (empty, gray symbols). The SDS concentrations in (a,c) and (b,d) are 8.4 and 70 mM, respectively. The corresponding $\langle r \rangle$ PDI from 0 to 800 s in (c,d) are plotted in the insets.

become thinner and large air bubbles form as a result of coalescence (Figures S5 and S6). The increased number of large air bubbles during this period leads to a higher bubble size polydispersity index (PDI) while $\langle r \rangle$ remains constant (Figure 6c,d). However, as a result of further thinning, film rupture occurs due to the insufficient elasticity of the foam film. Figure 6c,d shows an increase in both $\langle r \rangle_{t>400s}$ and $PDI_{t>400s}$, which is correlated to the transition points for ε at t > 400 s ($\varepsilon_{t>400s}$), whereby a faster decrease of the liquid fraction is observed due to coalescence, while the foam volume remains the same (Figure 5c,d). The effect of SDS concentration on ε, $\langle r \rangle$, and PDI of the given foams (from SDS solutions, fiber dispersions in SDS, and $Leachate_{SDS}$) is not significant at SDS concentrations above the cmc_{SDS}. The PDI was recorded until 800 s because of the small number of bubbles in the CSA, given their larger bubble size (Figures S5 and S6 at 1600 s). Therefore, the PDI derived from images at 1600 s are not meaningful.

CONCLUSIONS

The anionic surfactant (SDS) releases non-cellulosic components from wood fibers, including lignin, extractives, and possibly hemicellulose-bound species. The release of the non-cellulosics is speculated to be facilitated by fiber swelling, an effect that is not observed when cationic or nonionic surfactants are used. Our experimental results confirm the generation of surface-active aggregates, $Leachate_{0.7mM\ SDS}$, which are formed between non-cellulosics and SDS unimers via nonelectrostatic interactions. While the nature of the involved interactions and the formation of the leached aggregates are still open questions, it is interesting to note their distinctive effects in terms of surface activity. For instance, Leachate displays faster foamability compared to pure SDS solutions and fiber-loaded SDS solutions. Hence, for any given prospective application, we propose the use of anionic surfactants, or the respective leachate, to generate foams carrying suspended wood fibers. Such effects seem to be more evident in the case of mechanical or thermomechanical fibers (TMP), a subject that was also introduced in this study.

ASSOCIATED CONTENT

Supporting Information

The Supporting Information is available free of charge on the ACS Publications website at DOI: 10.1021/acs.biomac.9b00243.

Carbohydrates and extractive analysis; hydrodynamic size via dynamic light scattering; and surface activity of $Leachate_{0.7mM\ SDS}$ from other fiber sources (PDF)

Foam volume changes of $Leachate_{0.7mM\ SDS}$ from BKP fibers (AVI)

Foam volume changes of $Leachate_{0.7mM\ SDS}$ from 0.7 mM SDS over time (AVI)

AUTHOR INFORMATION

Corresponding Authors

*E-mail: cosima.stubenrauch@ipc.uni-stuttgart.de (C.S.).
*E-mail: orlando.rojas@aalto.fi (O.J.R.).

ORCID

Wenchao Xiang: 0000-0003-4281-3109

DOI: 10.1021/acs.biomac.9b00243
Biomacromolecules 2019, 20, 2286−2294

Blaise L. Tardy: 0000-0002-7648-0376
Cosima Stubenrauch: 0000-0002-1247-4006
Orlando J. Rojas: 0000-0003-4036-4020

Notes

The authors declare no competing financial interest.

■ ACKNOWLEDGMENTS

The H2020-ERC-2017-Advanced Grant "BioELCell" (788489) is acknowledged for funding support (O.J.R.). We are also thankful to the CLIC Innovation Ltd New Fibre Products project (https://clicinnovation.fi/projects/new-fiber-products/).

■ REFERENCES

(1) Dalgetty, L.; Kennedy, M. W. Building a home from foam-túngara frog foam nest architecture and three-phase construction process. *Biol. Lett.* **2010**, *6*, 293−296.
(2) Mira, I.; Andersson, M.; Boge, L.; Blute, I.; Carlsson, G.; Salminen, K.; Lappalainen, T.; Kinnunen, K. Foam Forming Revisited Part I. Foaming Behaviour of Fibre-Surfactant Systems. *Nord. Pulp Pap. Res. J.* **2014**, *29*, 679−688.
(3) Alimadadi, M.; Uesaka, T. 3D-Oriented Fiber Networks Made by Foam Forming. *Cellulose* **2016**, *23*, 661−671.
(4) Li, S.; Xiang, W.; Järvinen, M.; Lappalainen, T.; Salminen, K.; Rojas, O. J. Interfacial Stabilization of Fiber-Laden Foams with Carboxymethylated Lignin toward Strong Nonwoven Networks. *ACS Appl. Mater. Interfaces* **2016**, *8*, 19827−19835.
(5) Xiang, W.; Filpponen, I.; Saharinen, E.; Lappalainen, T.; Salminen, K.; Rojas, O. J. Foam Processing of Fibers As a Sustainable Alternative to Wet-Laying: Fiber Web Properties and Cause-Effect Relations. *ACS Sustain. Chem. Eng.* **2018**, *6*, 14423−14431.
(6) Huang, Z.; Su, M.; Yang, Q.; Li, Z.; Chen, S.; Li, Y.; Zhou, X.; Li, F.; Song, Y. A General Patterning Approach by Manipulating the Evolution of Two-Dimensional Liquid Foams. *Nat. Commun.* **2017**, *8*, 14110.
(7) Löbmann, K.; Wohlert, J.; Müllertz, A.; Wågberg, L.; Svagan, A. J. Cellulose Nanopaper and Nanofoam for Patient-Tailored Drug Delivery. *Adv. Mater. Interfaces* **2017**, *4*, 1600655.
(8) Patino, J. M. R.; Sánchez, C. C.; Niño, M. R. R. Implications of Interfacial Characteristics of Food Foaming Agents in Foam Formulations. *Adv. Colloid Interface Sci.* **2008**, *140*, 95−113.
(9) Drenckhan, W.; Saint-Jalmes, A. The Science of Foaming. *Adv. Colloid Interface Sci.* **2015**, *222*, 228−259.
(10) Hill, C.; Eastoe, J. Foams: From Nature to Industry. *Adv. Colloid Interface Sci.* **2017**, *247*, 496−513.
(11) Saint-Jalmes, A. Physical Chemistry in Foam Drainage and Coarsening. *Soft Matter* **2006**, *2*, 836−849.
(12) Derikvand, Z.; Riazi, M. Experimental Investigation of a Novel Foam Formulation to Improve Foam Quality. *J. Mol. Liq.* **2016**, *224*, 1311−1318.
(13) Martin, A.; Grolle, K.; Bos, M.; Stuart, M.; Vanvliet, T. Network Forming Properties of Various Proteins Adsorbed at the Air/Water Interface in Relation to Foam Stability. *J. Colloid Interface Sci.* **2002**, *254*, 175−183.
(14) Lam, S.; Velikov, K. P.; Velev, O. D. Pickering Stabilization of Foams and Emulsions with Particles of Biological Origin. *Curr. Opin. Colloid Interface Sci.* **2014**, *19*, 490−500.
(15) Beatrice, C. A. G.; Rosa-Sibakov, N.; Lille, M.; Sözer, N.; Poutanen, K.; Ketoja, J. A. Structural Properties and Foaming of Plant Cell Wall Polysaccharide Dispersions. *Carbohydr. Polym.* **2017**, *173*, 508−518.
(16) Song, J.; Chen, C.; Wang, C.; Kuang, Y.; Li, Y.; Jiang, F.; Li, Y.; Hitz, E.; Zhang, Y.; Liu, B.; Gong, A.; Bian, H.; Zhu, J. Y.; Zhang, J.; Li, J.; Hu, L. Superflexible Wood. *ACS Appl. Mater. Interfaces* **2017**, *9*, 23520−23527.
(17) Song, J.; Chen, C.; Zhu, S.; Zhu, M.; Dai, J.; Ray, U.; Li, Y.; Kuang, Y.; Li, Y.; Quispe, N.; Yao, Y.; Gong, A.; Leiste, U. H.; Bruck, H. A.; Zhu, J. Y.; Vellore, A.; Li, H.; Minus, M. L.; Jia, Z.; Martini, A.; Li, T.; Hu, L. Processing Bulk Natural Wood into a High-Performance Structural Material. *Nature* **2018**, *554*, 224−228.
(18) Jia, C.; Chen, C.; Kuang, Y.; Fu, K.; Wang, Y.; Yao, Y.; Kronthal, S.; Hitz, E.; Song, J.; Xu, F.; Liu, B.; Hu, L. From Wood to Textiles: Top-Down Assembly of Aligned Cellulose Nanofibers. *Adv. Mater.* **2018**, *30*, 1801347.
(19) Svagan, A. J.; Samir, M. A. S. A.; Berglund, L. A. Biomimetic Foams of High Mechanical Performance Based on Nanostructured Cell Walls Reinforced by Native Cellulose Nanofibrils. *Adv. Mater.* **2008**, *20*, 1263−1269.
(20) Gordeyeva, K. S.; Fall, A. B.; Hall, S.; Wicklein, B.; Bergström, L. Stabilizing Nanocellulose-Nonionic Surfactant Composite Foams by Delayed Ca-Induced Gelation. *J. Colloid Interface Sci.* **2016**, *472*, 44−51.
(21) Cervin, N. T.; Johansson, E.; Benjamins, J.-W.; Wågberg, L. Mechanisms Behind the Stabilizing Action of Cellulose Nanofibrils in Wet-Stable Cellulose Foams. *Biomacromolecules* **2015**, *16*, 822−831.
(22) Cervin, N. T.; Andersson, L.; Ng, J. B. S.; Olin, P.; Bergström, L.; Wågberg, L. Lightweight and Strong Cellulose Materials Made from Aqueous Foams Stabilized by Nanofibrillated Cellulose. *Biomacromolecules* **2013**, *14*, 503−511.
(23) Svagan, A. J.; Benjamins, J.-W.; Al-Ansari, Z.; Shalom, D. B.; Müllertz, A.; Wågberg, L.; Löbmann, K. Solid cellulose nanofiber based foams - Towards facile design of sustained drug delivery systems. *J. Control. Release* **2016**, *244*, 74−82.
(24) Pease, J. K. Method for Improving Pulp Washing Efficiency. U.S. Patent 5,405,498 A, Feb 21, 1993.
(25) Silveira, M. H. L.; Morais, A. R. C.; Lopes, A. M. d. C.; Olekszyszen, D. N.; Bogel-Łukasik, R.; Andreaus, J.; Pereira Ramos, L. Current Pretreatment Technologies for the Development of Cellulosic Ethanol and Biorefineries. *ChemSusChem* **2015**, *8*, 3366−3390.
(26) Westbye, P.; Köhnke, T.; Glasser, W.; Gatenholm, P. The Influence of Lignin on the Self-Assembly Behaviour of Xylan Rich Fractions from Birch (*Betula pendula*). *Cellulose* **2007**, *14*, 603−613.
(27) Simmons, T. J.; Mortimer, J. C.; Bernardinelli, O. D.; Pöppler, A.-C.; Brown, S. P.; DeAzevedo, E. R.; Dupree, R.; Dupree, P. Folding of Xylan onto Cellulose Fibrils in Plant Cell Walls Revealed by Solid-State NMR. *Nat. Commun.* **2016**, *7*, 13902.
(28) Tardy, B. L.; Yokota, S.; Ago, M.; Xiang, W.; Kondo, T.; Bordes, R.; Rojas, O. J. Nanocellulose-surfactant interactions. *Curr. Opin. Colloid Interface Sci.* **2017**, *29*, 57−67.
(29) Paria, S.; Manohar, C.; Khilar, K. C. Adsorption of Anionic and Non-Ionic Surfactants on a Cellulosic Surface. *Colloids Surf., A* **2005**, *252*, 221−229.
(30) Tucker, I. M.; Petkov, J. T.; Penfold, J.; Thomas, R. K. How Electrolyte and Polyelectrolyte Affect the Adsorption of the Anionic Surfactant SDS onto the Surface of a Cellulose Thin Film and the Structure of the Cellulose Film. 1. Hydrophobic Cellulose. *Langmuir* **2012**, *28*, 10773−10780.
(31) Tucker, I. M.; Petkov, J. T.; Penfold, J.; Thomas, R. K. Interaction of the Anionic Surfactant SDS with a Cellulose Thin Film and the Role of Electrolyte and Poyelectrolyte. 2 Hydrophilic Cellulose. *Langmuir* **2012**, *28*, 10223−10229.
(32) Quennouz, N.; Hashmi, S. M.; Choi, H. S.; Kim, J. W.; Osuji, C. O. Rheology of Cellulose Nanofibrils in the Presence of Surfactants. *Soft Matter* **2016**, *12*, 157−164.
(33) Carrillo, C. A.; Saloni, D.; Lucia, L. A.; Hubbe, M. A.; Rojas, O. J. Capillary Flooding of Wood with Microemulsions from Winsor I Systems. *J. Colloid Interface Sci.* **2012**, *381*, 171−179.
(34) Carrillo, C. A.; Saloni, D.; Rojas, O. J. Evaluation of O/W Microemulsions to Penetrate the Capillary Structure of Woody Biomass: Interplay between Composition and Formulation in Green Processing. *Green Chem.* **2013**, *15*, 3377−3386.
(35) Nypelö, T.; Laine, C.; Aoki, M.; Tammelin, T.; Henniges, U. Etherification of Wood-Based Hemicelluloses for Interfacial Activity. *Biomacromolecules* **2016**, *17*, 1894−1901.

DOI: 10.1021/acs.biomac.9b00243
Biomacromolecules 2019, 20, 2286−2294

(36) Boos, J.; Drenckhan, W.; Stubenrauch, C. Protocol for Studying Aqueous Foams Stabilized by Surfactant Mixtures. *J. Surfactants Deterg.* **2013**, *16*, 1−12.
(37) Sjostrom, E. The Origin of Charge on Cellulosic Fibers. *Nord. Pulp Pap. Res. J.* **1989**, *4*, 90−93.
(38) Nihonyanagi, S.; Yamaguchi, S.; Tahara, T. Direct evidence for orientational flip-flop of water molecules at charged interfaces: a heterodyne-detected vibrational sum frequency generation study. *J. Chem. Phys.* **2009**, *130*, 204704.
(39) Clar, J. G.; Silvera Batista, C. A.; Youn, S.; Bonzongo, J.-C. J.; Ziegler, K. J. Interactive Forces between Sodium Dodecyl Sulfate-Suspended Single-Walled Carbon Nanotubes and Agarose Gels. *J. Am. Chem. Soc.* **2013**, *135*, 17758−17767.
(40) de Oliveira, E. M.; da Costa, R. F.; Sanchez, S. D. A.; Natalense, A. P. P.; Bettega, M. H. F.; Lima, M. A. P.; Varella, M. T. d. N. Low-Energy Electron Scattering by Cellulose and Hemicellulose Components. *Phys. Chem. Chem. Phys.* **2013**, *15*, 1682−1689.
(41) Kiratzis, N.; Faers, M.; Luckham, P. F. Depletion Flocculation of Particulate Systems Induced by Hydroxyethylcellulose. *Colloids Surf., A* **1999**, *151*, 461−471.
(42) Filho, G. R.; Landim, A.; Sousa, R. M. F.; Ribeiro, E. A. M.; Souza, F. R. B.; ASSUNÇÃO, R. M. N.; Vieira, J. G.; CERQUEIRA, D. Application of Cationic Hemicelluloses Produced from Corn Husk as Polyelectrolytes in Sewage Treatment. *Polim.: Cienc. Tecnol.* **2013**, *23*, 468−472.
(43) Christian, R. *Solvents and Solvent Effects in Organic Chemistry*; Wiley-VCH: Weinheim, Germany, 1988.
(44) Du, X.; Pérez-Boada, M.; Fernández, C.; Rencoret, J.; del Río, J. C.; Jiménez-Barbero, J.; Li, J.; Gutiérrez, A.; Martínez, A. T. Analysis of Lignin−carbohydrate and Lignin−lignin Linkages after Hydrolase Treatment of Xylan−lignin, Glucomannan−lignin and Glucan−lignin Complexes from Spruce Wood. *Planta* **2014**, *239*, 1079−1090.
(45) Nishimura, H.; Kamiya, A.; Nagata, T.; Katahira, M.; Watanabe, T. Direct Evidence for α Ether Linkage between Lignin and Carbohydrates in Wood Cell Walls. *Sci. Rep.* **2018**, *8*, 6538.
(46) Lawoko, M.; Henriksson, G.; Gellerstedt, G. Structural Differences between the Lignin−Carbohydrate Complexes Present in Wood and in Chemical Pulps. *Biomacromolecules* **2005**, *6*, 3467−3473.
(47) Balakshin, M.; Capanema, E.; Gracz, H.; Chang, H.-m.; Jameel, H. Quantification of lignin-carbohydrate linkages with high-resolution NMR spectroscopy. *Planta* **2011**, *233*, 1097−1110.
(48) Watanabe, T.; Ohnishi, J.; Yamasaki, Y.; Kaizu, S.; Koshijima, T. Binding-site analysis of the ether linkages between lignin and hemicelluloses in lignin-carbohydrate complexes by DDQ-oxidation. *Agric. Biol. Chem.* **1989**, *53*, 2233−2252.
(49) Yuan, T.-Q.; Sun, S.-N.; Xu, F.; Sun, R.-C. Characterization of Lignin Structures and Lignin-Carbohydrate Complex (LCC) Linkages by Quantitative13C and 2D HSQC NMR Spectroscopy. *J. Agric. Food Chem.* **2011**, *59*, 10604−10614.
(50) Laine, J.; Stenius, P.; Carlsson, G.; Strom, G. The effect of ECF and TCF bleaching on the surface chemical composition of kraft pulp as determined by ESCA. *Nord. Pulp Pap. Res. J.* **1996**, *11*, 201−210.
(51) Jäsberg, A.; Selenius, P.; Koponen, A. Experimental Results on the Flow Rheology of Fiber-Laden Aqueous Foams. *Colloids Surf., A* **2015**, *473*, 147−155.
(52) Stubenrauch, C.; Shrestha, L. K.; Varade, D.; Johansson, I.; Olanya, G.; Aramaki, K.; Claesson, P. Aqueous foams stabilized by n-dodecyl-β-d-maltoside, hexaethyleneglycol monododecyl ether, and their 1 : 1 mixture. *Soft Matter* **2009**, *5*, 3070−3080.
(53) Salonen, A.; In, M.; Emile, J.; Saint-Jalmes, A. Solutions of Surfactant Oligomers: A Model System for Tuning Foam Stability by the Surfactant Structure. *Soft Matter* **2010**, *6*, 2271−2281.

DOI: 10.1021/acs.biomac.9b00243
Biomacromolecules 2019, 20, 2286−2294